IBRACON Structures and Materials Journal
Revista IBRACON de Estruturas e Materiais

ORIGINAL ARTICLE

Moving mass/load speed influence on the structural dynamic response of a bridge

Influência da velocidade da massa/carga móvel na resposta dinâmica da estrutura de uma ponte

Rafael Costa da Hora[a]
Silvio de Souza Lima[a]
Sergio Hampshire de Carvalho Santos[a]

[a]Universidade Federal do Rio de Janeiro – UFRJ, Department of Structures, Rio de Janeiro, RJ, Brasil

Abstract: The increasing technological advance in the structural engineering field allows not only the design of better structures, but also the development of new methods. When it comes to bridges, more specifically, railway bridges, a special kind of attention is necessary since the dynamic nature of some external loads must be taken into account. In this study, the inertial effect caused on the structure by the moving vehicle is quantified and taken into consideration in the analyses, through the coupling of the vehicle mass matrix with the global mass matrix of the structure at each integration time step. The numerical dynamic analysis was performed by the LOADYN software, a computer program developed by the authors. The influence of the train speed on the structural dynamic response is analyzed. Comparisons between the structural responses with and without the vehicle inertial effect are made. The results show the importance of the inertial forces generated by the vehicle. Those forces must be taken into account, especially at higher speeds and mass ratios since they play an important role on the response magnitude and critical velocities.

Keywords: structural dynamics, railway bridges, moving mass, numerical solution, LOADYN.

Resumo: O crescente avanço tecnológico permite não só a concepção de estruturas cada vez mais sofisticadas e esbeltas, mas também a criação de novos métodos. No caso de pontes, uma análise mais robusta se faz necessária tendo em vista a complexidade dos carregamentos atuantes de natureza dinâmica. No presente trabalho, as forças inerciais geradas pelas massas dos veículos na estrutura são levadas em consideração, e seus efeitos quantificados, através do acoplamento das matrizes de massas dos veículos à matriz de massa global da estrutura a cada intervalo de integração. A análise dinâmica em questão foi realizada pelo programa LOADYN, ferramenta computacional desenvolvida pelos autores. A influência da velocidade de passagem do veículo na resposta dinâmica da estrutura é analisada. São feitas comparações entre as respostas estruturais com e sem a consideração das forças inerciais geradas pelo veículo. Tais forças não devem ser negligenciadas, especialmente a grandes velocidades e altas relações entre as massas do veículo e estrutura já que têm um papel imprescindível na magnitude da resposta e nas velocidades críticas.

Palavras-chave: análise dinâmica, massas móveis, pontes ferroviárias, solução numérica, LOADYN.

1 INTRODUCTION

The growing development of high-speed trains makes the inertial effects generated by the vehicle masses on the structure extremely relevant to the analyses. The consideration of such effect simply as static loads amplification coefficients leads to conservative results when it comes to design safety. On the other hand, for a more specific analysis

of the dynamic problem, the accounting of these effects is crucial and may even lead to more economical projects [1]. This conservative approach of the problem neglects the influence of vital structural properties that play important roles in the dynamic analysis, such as, the geometry of the structural system itself, natural frequencies of vibration, vibration modes, vehicle speed and vehicle mass. When dealing with specific cases, for instance, a structure subjected to high-speed trains, these properties become relevant as the vehicle speed increases and the ratio between the vehicle mass and the structure mass increases [2].

In the case of multiple vehicles [3], the dynamic loading induced by the travelling vehicles on the structure is sequential and repetitive by nature, which implies the existence of some forced external frequency of excitation [4]–[6]. When the induced load frequency is close to some natural frequency of the structure, the resonance phenomena may occur. This external frequency can be predicted, basically, by the vehicle speed and the length between consecutive axels of the vehicle [7]. This study divides the problem in two groups with different approaches to the solution, the moving load problem and the moving mass problem. The first one treats the vehicle as a concentrated moving load with speed v acting on the structure through time. In the case of a simply supported beam, the aforementioned approach allows closed form solutions. The other way of dealing with the problem is by treating the vehicle as a concentrated moving mass. In addition to the effect of the moving load problem, this approach includes the inertial effects generated by the moving mass on the structure [5]. Evidently, in order to deal with more complex structural geometry, boundary conditions and loads, a numerical approach of the problem is essential in both cases [8], [9]. More complex models may be formulated and implemented. For instance, the consideration of the rail irregularities which may be numerically generated by random noise functions. The train can also be modeled as a sub dynamic system of any complexity limited only by the available computational resources [10]. However, these approaches play a major role when the primary concern is focused on the vehicle response itself regarding, for instance, passenger comfort, vehicle vertical acceleration and fatigue analysis. A more complex vehicle does not, necessarily, affect the overall structural response in terms of displacement as seen in [7] and [11]. For those reasons only the moving load and moving mass models were addressed in this paper. Figure 1 illustrates the moving load model.
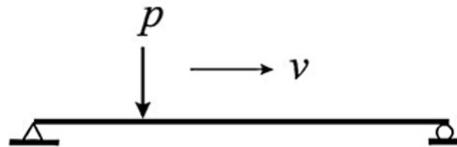
Figure 1. The moving load model.

As previously mentioned, this simplified model allows closed form solutions and is fundamentally governed by the Euler-Bernoulli differential equation, which constitutes the dynamic equilibrium of a beam (Equation 1).

$$m_b \frac{\partial^2 w(x,t)}{\partial t^2} + c \frac{\partial w(x,t)}{\partial t} + EI \frac{\partial^4 w(x,t)}{\partial x^4} = f(x,t) \tag{1}$$

Where, m_b is the linear mass, c the viscous damping coefficient, EI the flexural stiffness of the beam, $f(x,t)$ and $w(x,t)$ the externally applied loads and the deflection on the x coordinate on the instant t, respectively. When the vehicle inertial effects are considered, it is represented by a concentrated mass as shown in Figure 2.
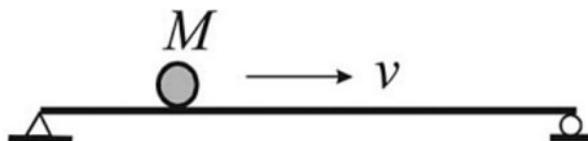
Figure 2. The moving mass model.

2 DESCRIPTION OF THE PROBLEM

This work aims to determine the influence of the vehicle speed on the structural dynamic response. More specifically, it aims to determine, quantify and compare the influence of the vehicle speed on the structure in the case of the moving load and the moving mass problem. Therefore, time history analyses are iteratively performed varying incrementally the vehicle travelling speed on each analysis. The maximum response values for each time history are stored. This process is called critical speed analysis [12]. The critical speeds are the ones that generate higher response magnitudes. The response comparison is achieved by plotting the relation between the structure and vehicle mass ratio against the vehicle speed on a 3D chart. The aforementioned process is used both for the moving load and moving mass problem.

3 METHODOLOGY

In order to perform the required analysis and solution visualization of the already described problems, a specific computational tool was entirely developed by the authors. The LOADYN software was built to solve the dynamic moving mass / load problem using 3D frame elements [13], [14]. Its capability was extended to perform modal analysis [15], [16], critical speed analysis and static analysis [17]. It uses a skyline storage scheme to efficiently manage memory resources when storing the system matrices [13] and a sparse solver to take advantage of the high level of sparsity of the system of equations. Therefore, a better performance is achieved by reducing the factorization time when solving the algebraic linear system of equations and by reducing the required memory for storage [18].

The unconditionally stable Newmark method was implemented to numerically solve the differential dynamic equilibrium equations of the problem [19], [20]. The inertial effects of the vehicle are taken into account by deriving a local mass matrix that represents the concentrated mass contributions at the element nodes and coupling it with the structure global mass matrix. This derived local matrix is called vehicle mass matrix [7]. As can be inferred by the nature of the problem, the vehicle mass matrix is not constant since it is a function of the vehicle position within the element domain. This can be regarded as a concentrated mass element as shown in Figure 3. This numerical approach allows the quantification of the vehicle inertial influence on the response for any structural geometry configuration and is not adopted by the available commercial softwares known by the authors.
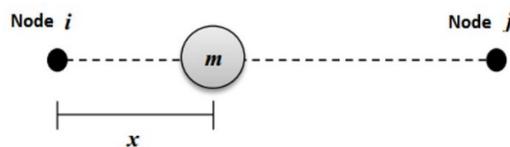
Figure 3. The concentrated mass element.

In Figure 3, x is the distance from the concentrated mass to the initial node of the element and m is the concentrated mass. The distance x increases in $v * \Delta t$ on each integration time step, where v is the vehicle speed and Δt is the chosen time step. Therefore, the vehicle mass matrix needs to be assembled on each solution time step since x is not constant. The derivation of the vehicle local mass matrix is given by the use of the element shape functions. There is no distributed mass within the concentrated mass element domain, which means there is no need for the usual integration process. Equation 2 synthesizes what was described.

$$[M] = [M_e] + \sum_{i=1}^{j}[N(x)]^T[m_i][N(x)] \tag{2}$$

Where, [M] is the sum of the element mass matrix with the vehicle mass matrix, $[M_e]$ is the element mass matrix, [N(x)] is the element shape functions in matrix form, $[m_i]$ is vehicle mass matrix and j is the number of vehicles within the element at time t.

3.1 THE SYSTEM MATRICES

The 3D uniform frame element stiffness matrix [k] used by the program is shown in Figure 4. The shear deformation is taken into account by the factors $Ö_y$ e $Ö_z$. The complete formulation of the stiffness matrix is presented in [21].

$$K = \begin{bmatrix}
\frac{EA}{l} \\
0 & \frac{12EI_z}{l^3(1+\Phi_y)} \\
0 & 0 & \frac{12EI_y}{l^3(1+\Phi_z)} \\
0 & 0 & 0 & \frac{GJ}{l} \\
0 & 0 & \frac{-6EI_y}{l^2(1+\Phi_z)} & 0 & \frac{(4+\Phi_z)EI_y}{l(1+\Phi_z)} \\
0 & \frac{6EI_z}{l^2(1+\Phi_y)} & 0 & 0 & 0 & \frac{(4+\Phi_y)EI_z}{l(1+\Phi_y)} \\
\frac{-EA}{l} & 0 & 0 & 0 & 0 & 0 & \frac{AE}{l} \\
0 & \frac{-12EI_z}{l^3(1+\Phi_y)} & 0 & 0 & 0 & \frac{-6EI_z}{l^2(1+\Phi_y)} & 0 & \frac{12EI_z}{l^3(1+\Phi_y)} \\
0 & 0 & \frac{-12EI_y}{l^3(1+\Phi_z)} & 0 & \frac{6EI_y}{l^2(1+\Phi_z)} & 0 & 0 & 0 & \frac{12EI_y}{l^3(1+\Phi_z)} \\
0 & 0 & 0 & \frac{-GJ}{l} & 0 & 0 & 0 & 0 & 0 & \frac{GJ}{l} \\
0 & 0 & \frac{-6EI_y}{l^2(1+\Phi_z)} & 0 & \frac{(2-\Phi_z)EI_y}{l(1+\Phi_z)} & 0 & 0 & 0 & \frac{6EI_y}{l^2(1+\Phi_z)} & 0 & \frac{(4+\Phi_z)EI_y}{l(1+\Phi_z)} \\
0 & \frac{6EI_z}{l^2(1+\Phi_y)} & 0 & 0 & 0 & \frac{(2-\Phi_y)EI_z}{l(1+\Phi_y)} & 0 & \frac{-6EI_z}{l^2(1+\Phi_y)} & 0 & 0 & 0 & \frac{(4+\Phi_y)EI_z}{l(1+\Phi_y)}
\end{bmatrix}$$

(Symmetric)

Figure 4. Element stiffness matrix.

The consistent element mass matrix $[M_e]$ with rotational inertia is used by the software instead of the lumped one. The 3D uniform frame element mass matrix is shown in Figure 5. Its complete formulation is also presented in [21].

$$m = \rho A l \begin{bmatrix}
\frac{1}{3} \\
0 & \frac{13}{35}+\frac{6I_z}{5Al^2} \\
0 & 0 & \frac{13}{35}+\frac{6I_y}{5Al^2} \\
0 & 0 & 0 & \frac{J_x}{3A} \\
0 & 0 & -\frac{11l}{210}-\frac{I_y}{10Al} & 0 & \frac{l^2}{105}+\frac{2I_y}{15A} \\
0 & \frac{11l}{210}+\frac{I_z}{10Al} & 0 & 0 & 0 & \frac{l^2}{105}+\frac{2I_z}{15A} \\
\frac{1}{6} & 0 & 0 & 0 & 0 & 0 & \frac{1}{3} \\
0 & \frac{9}{70}-\frac{6I_z}{5Al^2} & 0 & 0 & 0 & \frac{13l}{420}-\frac{I_z}{10Al} & 0 & \frac{13}{35}+\frac{6I_z}{5Al^2} \\
0 & 0 & \frac{9}{70}-\frac{6I_y}{5Al^2} & 0 & -\frac{13l}{420}+\frac{I_y}{10Al} & 0 & 0 & 0 & \frac{13}{35}+\frac{6I_y}{5Al^2} \\
0 & 0 & 0 & \frac{J_x}{6A} & 0 & 0 & 0 & 0 & 0 & \frac{J_x}{3A} \\
0 & 0 & \frac{13l}{420}-\frac{I_y}{10Al} & 0 & -\frac{l^2}{140}-\frac{I_y}{30A} & 0 & 0 & 0 & \frac{11l}{210}+\frac{I_y}{10Al} & 0 & \frac{l^2}{105}+\frac{2I_y}{15A} \\
0 & -\frac{13l}{420}+\frac{I_z}{10Al} & 0 & 0 & 0 & -\frac{l^2}{140}-\frac{I_z}{30A} & 0 & -\frac{11l}{210}-\frac{I_z}{10Al} & 0 & 0 & 0 & \frac{l^2}{105}+\frac{2I_z}{15A}
\end{bmatrix}$$

(Symmetric)

Figure 5. Element mass matrix.

The Rayleigh formulation was adopted for the system damping, which means that [C], the global damping matrix, is a linear combination of [K] and [M], the global stiffness and mass matrix, respectively.

$$[C] = \alpha[M] + \beta[K] \tag{3}$$

where,

$$\alpha = 2\omega_k \frac{\xi_k \omega_i^2 - \xi_i \omega_i \omega_k}{\omega_i^2 - \omega_k^2} \tag{4}$$

$$\beta = \frac{2\xi_i \omega_i - 2\xi_k \omega_k}{\omega_i^2 - \omega_i \omega_k} \tag{5}$$

In this case, ω_i and ω_k are the frequency range limits relevant to the analysis. They may or may not match some of the structure's natural frequencies. ξ_i and ξ_k represent the damping ratios of the structure for i and k frequencies A diagram of the Rayleigh damping is shown in Figure 6.
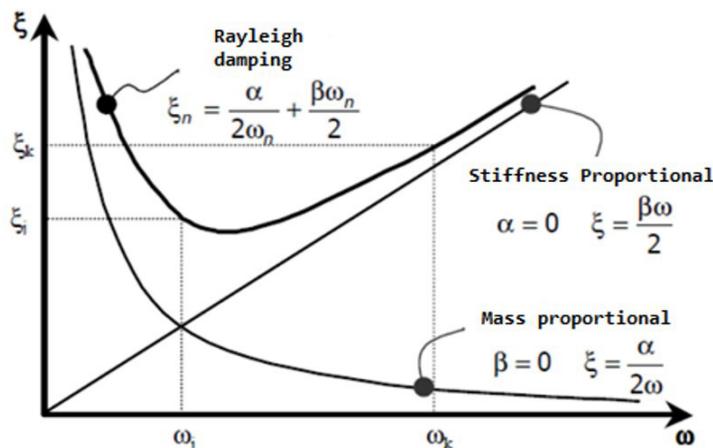
Figure 6. Rayleigh damping.

3.2 DYNAMIC INTERACTION MODELING

The dynamic interaction was taken into account through the contact points between vehicle and structure. Despite the vehicle is not treated as a dynamic system in this work, the following approach of the problem allows the implementation of the vehicle matrices if desired. In other words, the vehicle representation can vary from a single moving load to a complex chain of multiple coupled dynamic systems. The contact points cause the coupling of the differential equations in the problem. The assembled matrices are time dependent and must be updated as the contact points change position. It defines an incremental time history analysis. [19] explains the Newmark method for linear systems, a consolidated, implicit and unconditionally stable numerical method used to direct integrate the dynamic equilibrium equations.

The vehicle may be divided into two parts: the upper or noncontact part consists of the car body, suspension systems and bogies which DOF's are indicated by the vector $\{d_u\}$. The wheel or contact part consists of the wheelsets. Assuming that each wheelset is represented by one vertical DOF, the wheel part can be denoted as $\{d_w\}$. The vehicle equilibrium equation:

$$[m_v]\{\ddot{d}_v\} + [c_v]\{\dot{d}_v\} + [k_v]\{d_v\} = \{f_v\} \tag{6}$$

Rev. IBRACON Estrut. Mater., vol. 16, no. 6, e16601, 2023

5/18

Where the force vector $\{f_v\}$ may be split as follows:

$$\{f_v\} = \{f_e\} + [l]\{f_c\} \tag{7}$$

The vector $\{f_e\}$ represents the external forces except the contact ones, which are represented by the vector $\{f_c\}$. $[l]$ is a transformation matrix. The displacement vector $\{d_v\}$ is composed by $\langle\{d_u\}\{d_w\}\rangle^T$, which represent the displacements in the direction of the degrees of freedom without and with contact with the structure, respectively. The wheels displacements $\{d_w\}$ are connected to the contact points displacements $\{d_c\}$ through the following relation:

$$\{d_w\} = [\tilde{A}]\{d_c\} + \{r\} \tag{8}$$

The $[\tilde{A}]$ matrix represents the vehicle jumping conditions and assumes unitary value if no jumps exist in the analysis. $\{r\}$ vector accounts for the rail irregularities. When those are not considered, the wheels displacements and the contact points displacements are the same. Only the contact forces acting towards gravity direction are taken into account within the context of this work. Horizontal forces generated by breaking are not studied.

The analysis takes into consideration that all the information of the system on time t are known. A small integration time step value $\ddot{A}t$ is assigned. The analysis interest lies on obtaining the system responses for time $t + \ddot{A}t$. Equation 6 can be rewritten in matrix form for the new integration time step separating the vehicle degrees of freedom and the wheels (contact) degrees of freedom as follows:

$$\begin{bmatrix}[m_{uu}] & [m_{uw}]\\ [m_{wu}] & [m_{ww}]\end{bmatrix}\begin{Bmatrix}\{\ddot{d}_u\}\\ \{\ddot{d}_w\}\end{Bmatrix}_{t+\ddot{A}t} + \begin{bmatrix}[c_{uu}] & [c_{uw}]\\ [c_{wu}] & [c_{ww}]\end{bmatrix}\begin{Bmatrix}\{\dot{d}_u\}\\ \{\dot{d}_w\}\end{Bmatrix}_{t+\ddot{A}t} + \begin{bmatrix}[k_{uu}] & [k_{uw}]\\ [k_{wu}] & [k_{ww}]\end{bmatrix}\begin{Bmatrix}\{d_u\}\\ \{d_w\}\end{Bmatrix}_{t+\ddot{A}t} = \begin{Bmatrix}\{f_{ue}\}\\ \{f_{we}\}\end{Bmatrix}_{t+\ddot{A}t} + \begin{bmatrix}[l_u]\\ [l_w]\end{bmatrix}\{f_c\}_{t+\ddot{A}t} \tag{9}$$

Expanding equation's 9 first line:

$$[m_{uu}]\{\ddot{d}_u\}_{t+\ddot{A}t} + [c_{uu}]\{\dot{d}_u\}_{t+\ddot{A}t} + [k_{uu}]\{d_u\}_{t+\ddot{A}t} = \{f_{ue}\}_{t+\ddot{A}t} - \{q_{uc}\}_{t+\ddot{A}t} \tag{10}$$

Where,

$$\{q_{uc}\}_{t+\ddot{A}t} = [m_{uw}]\{\ddot{d}_w\}_{t+\ddot{A}t} + [c_{uw}]\{\dot{d}_w\}_{t+\ddot{A}t} + [k_{uw}]\{d_w\}_{t+\ddot{A}t} \tag{11}$$

Applying the Newmark's method described in [19] and some algebraic transformation as shown in [7], part of the solution is obtained as follows:

$$\{\ddot{d}_u\}_{t+\ddot{A}t} = b_0\{\ddot{A}d_u\} - b_1\{\dot{d}_u\}_t - b_2\{\ddot{d}_u\}_t \ ;$$

$$\{\dot{d}_u\}_{t+\ddot{A}t} = \{\dot{d}_u\}_t + b_3\{\ddot{d}_u\}_t + b_4\{\ddot{d}_u\}_{t+\ddot{A}t} \ ; \tag{12}$$

$$\{d_u\}_{t+\ddot{A}t} = \{d_u\}_t + \{\ddot{A}d_u\} \ ;$$

The parameters for the solution's numerical stability $\beta\ and\ \gamma$; and the coefficients above are:

$$b_0 = \frac{1}{\beta \ddot{A}t^2} \; ; \; b_1 = \frac{1}{\beta \ddot{A}t} \; ; \; b_2 = \frac{1}{2\beta} - 1 \; ;$$
$$b_3 = (1 - \gamma)\ddot{A}t \; ; \; b_4 = \gamma \ddot{A}t \; ; \; b_5 = \frac{\gamma}{\beta \ddot{A}t} \; ;$$
$$b_6 = \frac{\gamma}{\beta} - 1 \; ; \; b_7 = \frac{\ddot{A}t}{2}\left(\frac{\gamma}{\beta} - 2\right) ;$$
$$\gamma = \frac{1}{2} \; ; \; \beta = \frac{1}{4} \; ;$$

(13)

Plugging in Equation 12 into Equation 9 with the necessary algebraic manipulation, the solution can proceed by solving a linear system of algebraic equation:

$$[\emptyset_{uu}]\{\ddot{A}d_u\} = \{f_{ue}\}_{t+\ddot{A}t} - \{q_{uc}\}_{t+\ddot{A}t} + \{q_u\}_t$$

(14)

Where,

$$[\emptyset_{uu}] = b_0[m_{uu}] + b_5[c_{uu}] + [k_{uu}]$$

(15)

And,

$$\{q_u\}_t = [m_{uu}]\left(b_1\{\dot{d}_u\}_t + b_2\{\ddot{d}_u\}_t\right)$$

$$+[c_{uu}]\left(b_6\{\dot{d}_u\}_t + b_7\{\ddot{d}_u\}_t\right) - [k_{uu}]\{d_u\}_t$$

(16)

The solution of the algebraic linear system represents the displacement increments $\{\ddot{A}d_u\}$ of the vehicle's degrees of freedom not in contact with the structure. Plugging in this vector in the Equation 12, the displacement vector $\{d_u\}_{t+\ddot{A}t}$ of the upper part is achieved. When these displacements are known for the $t + \ddot{A}t$ time step, the contact forces acting on the system are easily obtained by the substitution of these displacements in the governing Equation 9 of the problem. Expanding the second line terms of this equation as follows:

$$\{f_c\}_{t+\ddot{A}t} = [m_c]\{\ddot{d}_w\}_{t+\ddot{A}t} + [c_c]\{\dot{d}_w\}_{t+\ddot{A}t} + [k_c]\{d_w\}_{t+\ddot{A}t} + \{p_c\}_{t+\ddot{A}t} + \{q_c\}_t$$

(17)

Where the contact matrices are:

$$[m_c] = [l_w]^{-1}([m_{ww}] - [\emptyset_{wu}][\emptyset_{uu}]^{-1}[m_{uw}]) \; ;$$

$$[c_c] = [l_w]^{-1}([c_{ww}] - [\emptyset_{wu}][\emptyset_{uu}]^{-1}[c_{uw}]) \; ;$$

(18)

$$[k_c] = [l_w]^{-1}([k_{ww}] - [\emptyset_{wu}][\emptyset_{uu}]^{-1}[k_{uw}]) \; ;$$

The load vectors are:

$$\{p_c\}_{t+\ddot{A}t} = [l_w]^{-1}([\emptyset_{wu}][\emptyset_{uu}]^{-1}\{f_{ue}\}_{t+\ddot{A}t} - \{f_{we}\}_{t+\ddot{A}t})$$

$$\{q_c\}_t = [l_w]^{-1}([\emptyset_{wu}][\emptyset_{uu}]^{-1}\{q_u\}_t - \{q_w\}_t)$$

(19)

In addition,

Rev. IBRACON Estrut. Mater., vol. 16, no. 6, e16601, 2023

7/18

$$[\emptyset_{wu}] = b_0[m_{wu}] + b_5[c_{wu}] + [k_{wu}] \tag{20}$$

$$\{q_w\}_t = [m_{wu}]\left(b_1\{\dot{d}_u\}_t + b_2\{\ddot{d}_u\}_t\right)$$

$$+[c_{wu}]\left(b_6\{\dot{d}_u\}_t + b_7\{\ddot{d}_u\}_t\right) - [k_{wu}]\{d_u\}_t \tag{21}$$

Since no jump conditions are allowed, the wheels displacements are treated as the contact displacements, which means $\{d_w\} \equiv \{d_c\}$. Therefore, Equation 17 may be rewritten as follows:

$$\{f_c\}_{t+\Delta t} = [m_c]\{\ddot{d}_c\}_{t+\Delta t} + [c_c]\{\dot{d}_c\}_{t+\Delta t} + [k_c]\{d_c\}_{t+\Delta t} + \{p_c\}_{t+\Delta t} + \{q_c\}_t \tag{22}$$

3.2.1 THE NEWMARK METHOD

Newmark's direct integration process is widely used for numerical solution of systems of differential equations, mainly when it comes to structural dynamics and wave propagation, for instance. The numerical stability of its solution does not depend on the size of the chosen integration time step. That is why the method is unconditionally stable. This does not mean, however, that the mathematical solution accuracy does not depend on the numerical step size. It is an implicit method. In other words, it is mandatory to know the state of all variables of the problem on the previous step in order to achieve its equilibrium conditions. Generally speaking, implicit methods have lower computational costs and the solutions are more robust when compared to explicit methods [20]. The average acceleration method was implemented in the present work.

3.2.2 THE MOVING MASS ALGORITHM

The main analysis algorithm is synthetized and presented as a pseudocode in table 1. The user is able to opt for the account of the vehicle inertial effect in the analysis by simply setting the VEHICLE_INERTIAL_EFFECT key to *TRUE* [12]. The algorithm returns the degrees of freedom displacements, velocities and accelerations for all the integration time steps. The time history response solution may now be visualized and internal stresses calculated.

Table 1. Main algorithm pseudocode

```
ALGORITHM: MAIN ANALYSIS
1   PROGRAM MAIN
2   FOR I:= 1 TO NUMBER_OF_TIME_STEPS DO:
3     FOR W:= 1 TO NUMBER_OF_VEHICLE_LOADS DO:
4       X[W]:= UPDATE_LOAD_POSITION()
5       IF X[W] IS_ON_THE_STRUCTURE THEN:
6         E[W]:= CHECKS_CONTACT_ELEMENT_NUMBER()
7         F[W]:= ELEMENT_NODAL_FORCES_VECTOR()
8         ADD_TO_GLOBAL_FORCES_VECTOR(F[W])
9         IF VEHICLE_INERTIAL_EFFECT == TRUE THEN:
10          M:= ASSEMBLE_VEHICLE_LOAD_MASS_MATRIX(E[W],X[W])
11          UPDATE_GLOBAL_MASS_MATRIX(M)
12        END IF 9
13      END IF 5
14    END FOR 3
15    FL : = ASSEMBLE_NEWMARK_PSEUDOFORCE_VECTOR()
16    KL : = ASSEMBLE_NEWMARK_PSEUDOSTIFFNESS_MATRIX()
17    U[:, I]:= SOLVE_NEWMARK_PSEUDOSYSTEM_FOR_DISPLACEMENT(FL,KL)
18    V[:, I]:= CALCULATE_VELOCITY()
19    A[:, I]:= CALCULATE_ACCELERATION()
20  END FOR 2
21  RETURN(U,V,A)
22
23  END MAIN
```

4 CASE STUDY

4.1 SINGLE MOVING MASS
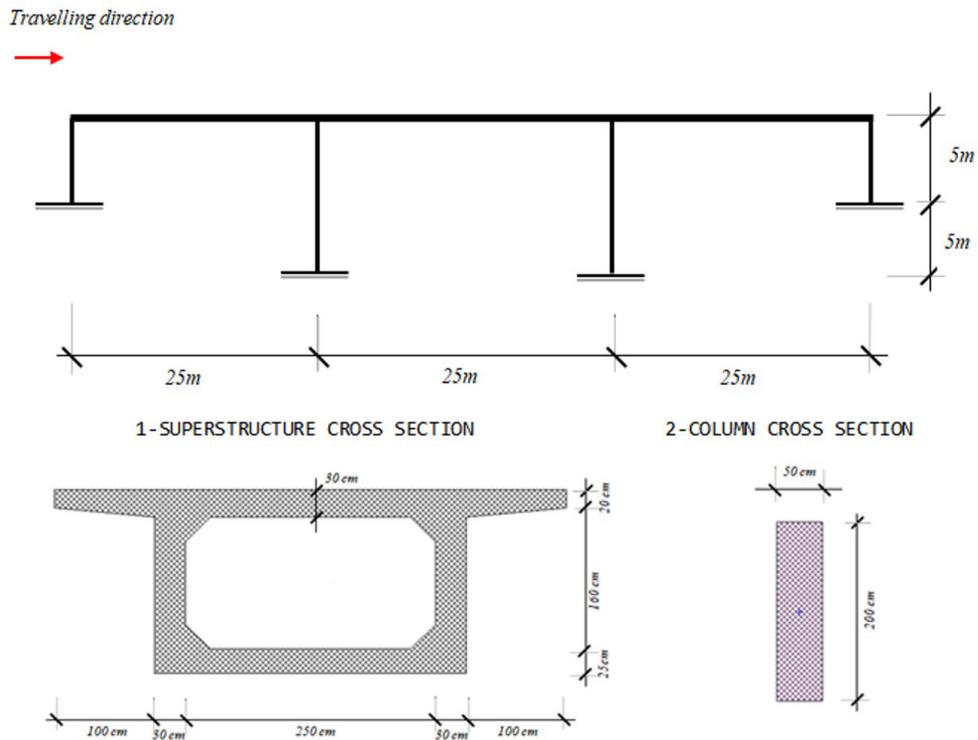
Figure 7. The structural model.

The structural model and the cross sections used in the analysis are shown in Figure 7. The material and properties of the structural model are presented in Table 2.

Table 2. Material and section properties [kN, m].

MATERIAL PROPERTIES						
Num	E	Poisson	Alpha	Gamma		
1	28E+06	0.2	1E+05	25.0		
SECTION PROPERTIES						
Num	Ax	Ay	Az	Ix	Iy	Iz
1	3.1	0.0	0.0	2.96	5.16	1.51
2	1	0.0	0.0	0.07	0.33	0.021

Where, E is the Young's modulus, Gamma is the specific weight of the material, A the cross-sectional area, I_y and I_z the second moment of area, I_x the torsional constant of the section, *Alpha* and *Gamma* are the material thermal expansion coefficient and the specific weight, respectively, A_y and A_z represent the shear areas (the effective area of the section participating in the shear deformation). The model is then pre-processed by the software as shown in Figure 8. The discrete model is represented by 20 elements and 126 degrees of freedom. The element consistent mass matrix was implemented in order to better represent the mass distribution within its domain. Figure 9 shows the moving mass analysis input data from the software's editor. The analysis properties shown were changed throughout the process.
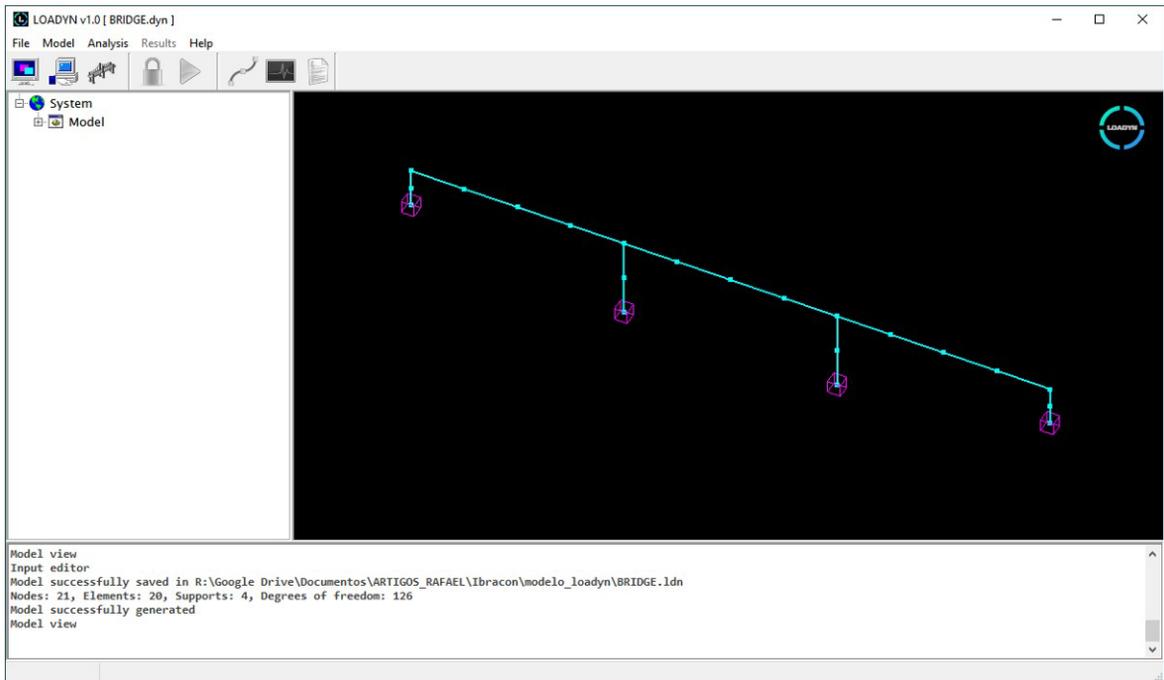
Figure 8. Pre-processed model.

Figure 9. Analysis input data.

The structure mass used to compute the mass ratio (vehicle/bridge) was the superstructure mass between columns (middle free span). In this section a single moving load/mass was considered.

4.2 MULTIPLE MOVING MASSES

This section prepares the analyses to compare the results of the critical speed analysis for the multiple moving loads and masses problems using the same structural model.
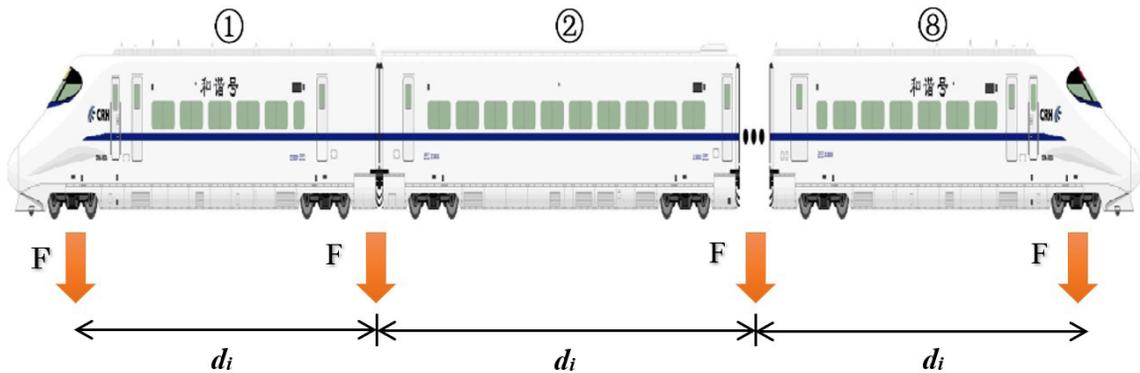
Figure 10. Axle arrangements of high speed train model.

Figure 10 shows a schematic representation of the vehicle. The train is modeled by multiple forces F (axles) equally spaced by d_i. It consists of 8 cars with the length of 25m each. In summary, the entire vehicle is modeled by 9 loads of 125 kN each. The critical speed analysis input data for vehicle speed was 10 m/s as starting speed to 150m/s as final speed. The vehicle speed was incremented 200 times between the defined speed limits. The critical speed analysis process was presented in section 2 of this study.

5 RESULTS AND DISCUSSIONS

5.1 SINGLE MOVING MASS CASE

The analyses are iteratively performed in order to gather enough data. For each performed analysis the bridge maximum absolute vertical displacement of the central node and the mass ratio are stored. The comparison results are presented in Figure 11. The first one compares the structure absolute maximum displacement values obtained by the moving mass and moving load analyses for different mass ratios. The second one compares the relative difference between the structure absolute maximum displacement values obtained by the moving mass and moving load analyses.
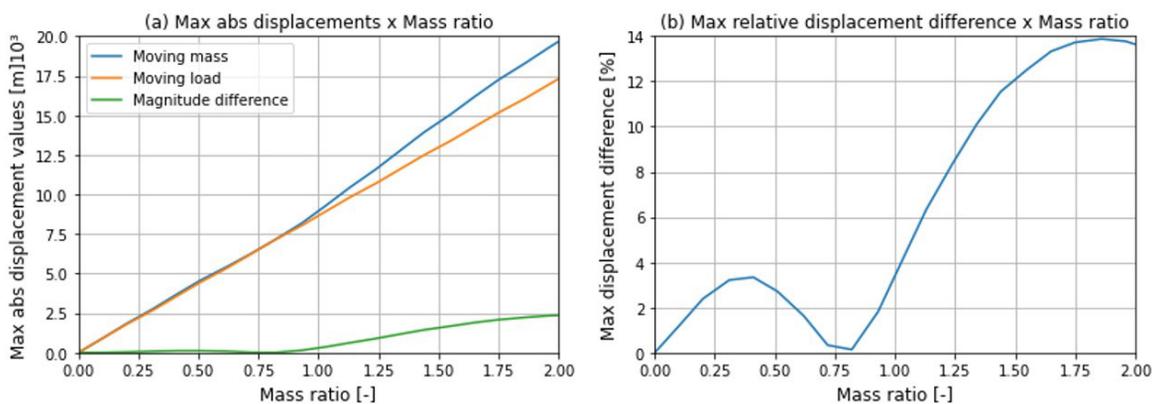
Figure 11. (a) Absolute and (b) relative difference between analysis max responses.

Figure 11 shows the difference between the moving mass analyses and the moving load analyses responses maximum absolute and relative values. For this case study, as shown, the responses difference only has significant

Rev. IBRACON Estrut. Mater., vol. 16, no. 6, e16601, 2023

11/18

values when the mass ratio becomes greater than approximately one. In other words, the vehicle inertial effect plays a non-negligible role in the analysis when the vehicle mass is greater than the structure mass in terms of magnitude. Figure 12 shows and compares the time history responses of both moving mass and moving load analysis for different mass ratios.
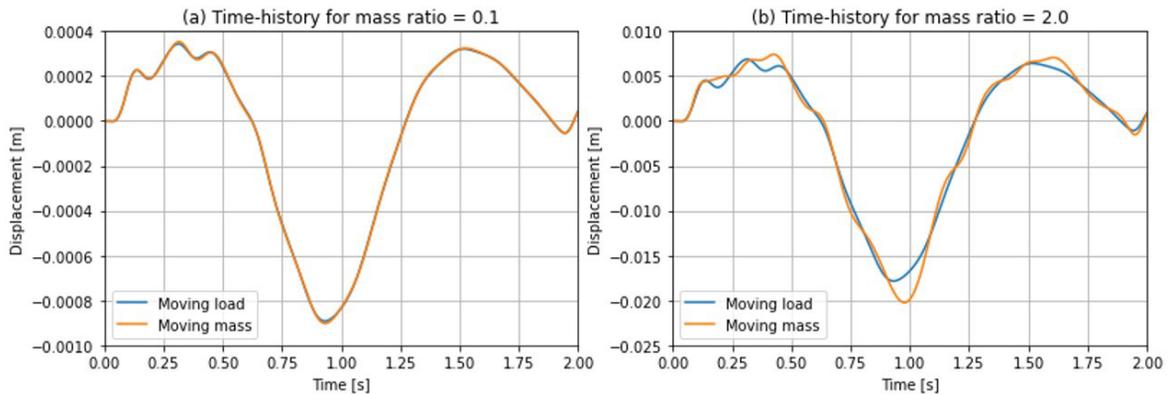
Figure 12. (a) Time-history for mass ratio = 0.1 (b) Time-history for mass ratio = 2.0.

From chart (a) on Figure 12, it is clear that the absolute displacement difference between analyses types is almost inexistent from an engineering point of view. Chart (b), visually shows clear absolute magnitude difference between responses. This magnitude difference is measured and presented on Figure 13 in absolute terms over time.
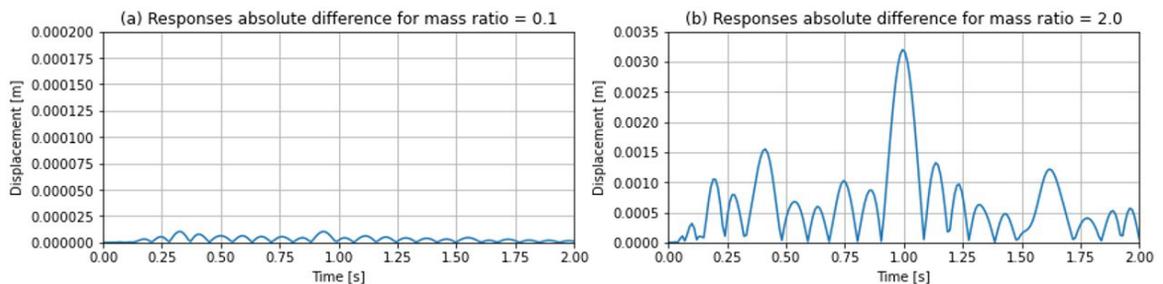
Figure 13. (a) Time-history absolute difference for mass ratio = 0.1 (b) Time-history absolute difference for mass ratio = 2.0.

The absolute magnitude time-history difference between analyses is not only visually, but quantitatively confirmed. As already discussed, for a low mass ratio the difference between analyses is negligible from an engineering perspective. Notice that Figure 13a and b do not share the same order of magnitude on the ordinate axis scale. In some cases, the relative difference is also important as shown next.
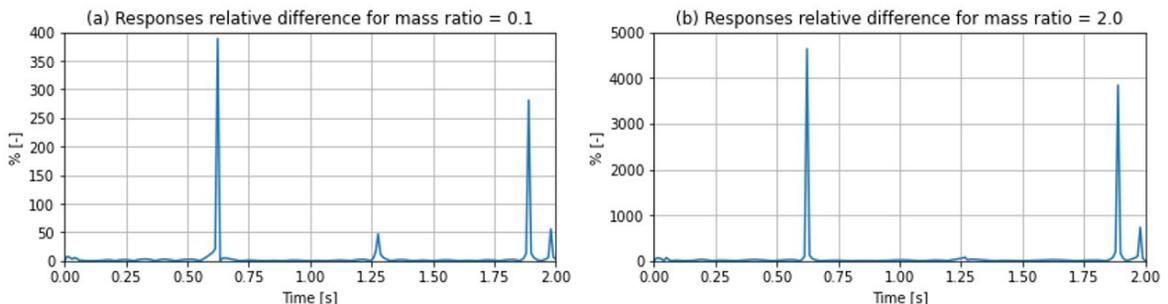
Figure 14. (a) Time-history relative difference for mass ratio = 0.1 (b) Time-history relative difference for mass ratio=2.0.

Figure 13 and 14 demonstrate that the greater relative differences do not necessarily occur at the same point in time where the biggest absolute differences occur. This in turn does not mean that the relative differences are necessarily bigger than the absolute ones. The relative differences peaks occur when time-history values get close to zero.

Ultimately, the relation between the structure and vehicle mass ratio and the vehicle speed is plotted against the maximum structural response on the same degree of freedom for the given moving load and the moving mass situation. Figures 15 and 16 show the structural response tendency across the analyzed dimensions for the moving load and moving mass problem, respectively. The former shows a linear variation of the response throughout the mass ratio axis for any given velocity. On the other hand, when observed from the velocity axis, the response assumes a specific shape which is entirely linearly amplified for any increasing mass ratio. The response peaks often indicate resonance condition and should be avoided. The latter shows an indirect behavior of the response across any analyzed dimension. In addition, for any increasing variation of mass ratio at any given velocity, a non-linear growth of the response can be noticed. Figures 17 and 18 feature the contour plots of the discussed situations in order to provide, perhaps, a better comprehension of the general behavior of the moving load/mass problem.
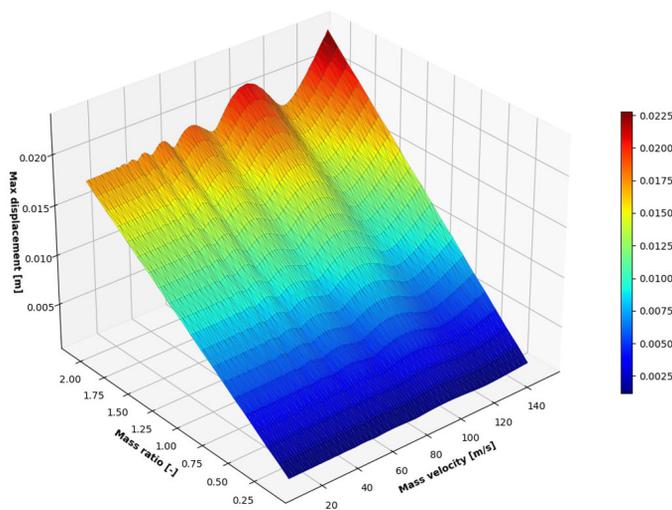
Figure 15. 3D Plot for the moving load problem.
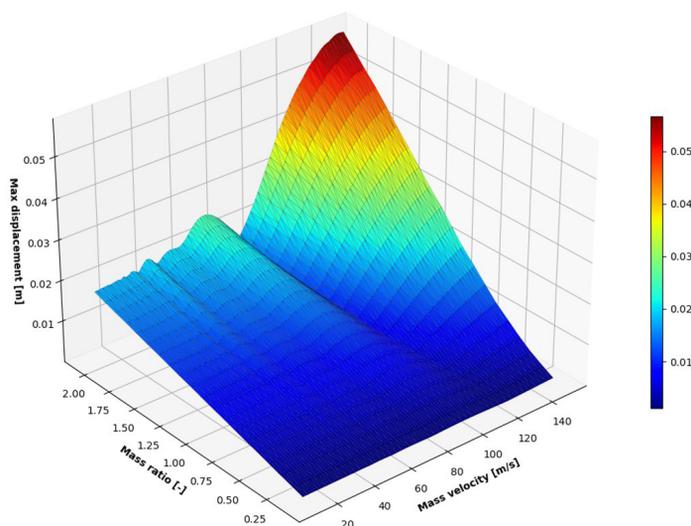
Figure 16. 3D Plot for the moving mass problem.

Figure 15 clearly shows the increasing direct response shape tendency across the mass ratio dimension as presented. In Figure 16, the response peaks appear to be left shifted as the mass ratio grows. This configures a decrease in resonance velocities as the mass ratio increases. In other words, the greater the mass present on the structure, the lower the dynamic natural frequency of the entire system. Consequently, a lower travelling vehicle velocity is required to generate critical structural responses. That justifies the left shifted response peaks.
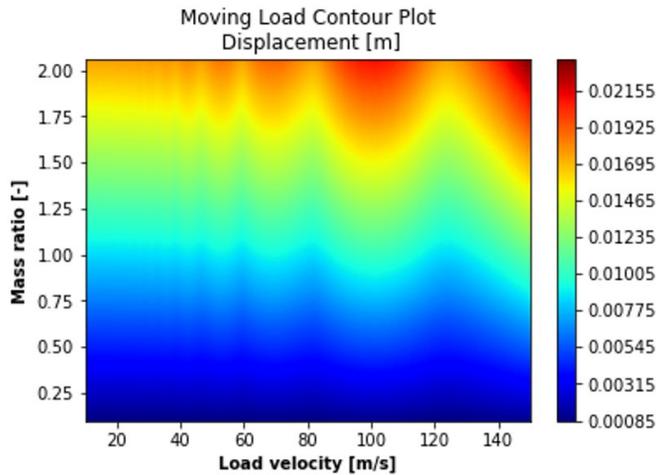
Figure 17. Contour Plot for the moving load problem.
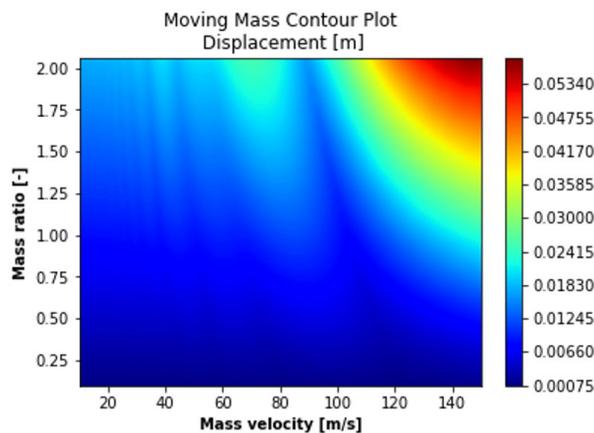
Figure 18. Contour Plot for the moving mass problem

5.2 MULTIPLE MOVING MASSES CASE

First, different time history responses are presented for the multiple moving masses scenario. Figure 19 shows the midpoint vertical displacements time-histories for a vehicle travelling speed of 10 m/s with an integration time step $\Delta t = 0.01$s and a vehicle travelling speed of 150 m/s with an integration time step $\Delta t = 7 \cdot 10^{-4} s$. Figure 20 shows the acceleration time-histories based on the same parameters mentioned for Figure 19.
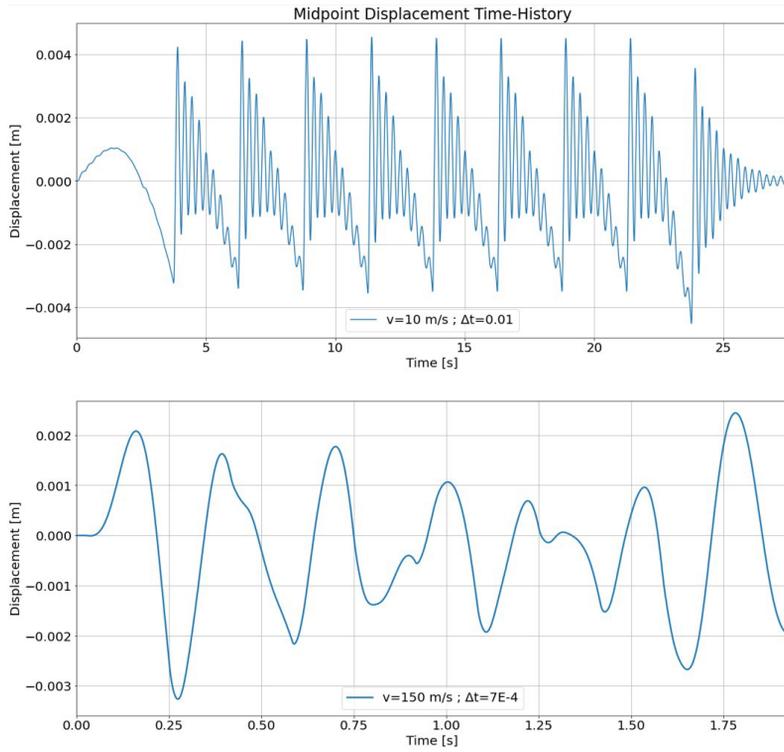
Figure 19. Displacement time-history
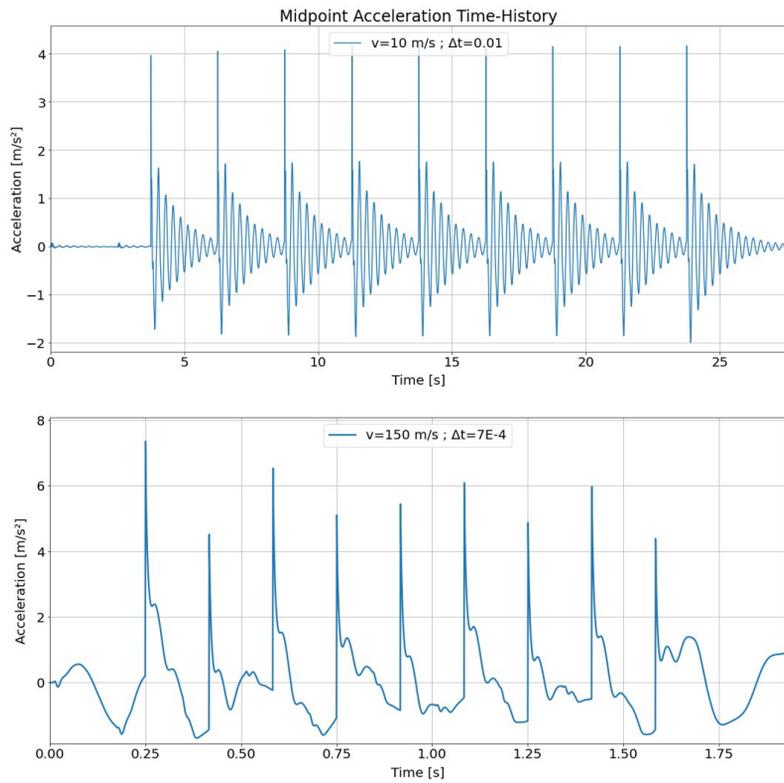
Figure 20. Acceleration time-history

These analyses were performed in order to better simulate real design situations with multiple moving masses acting simultaneously on the structure. Critical speed analysis for the multiple moving loads and multiple moving masses cases were also performed and compared as follows. Figure 21 shows that the greater response peak occurs at a vehicle travelling speed of approximately 90 m/s.
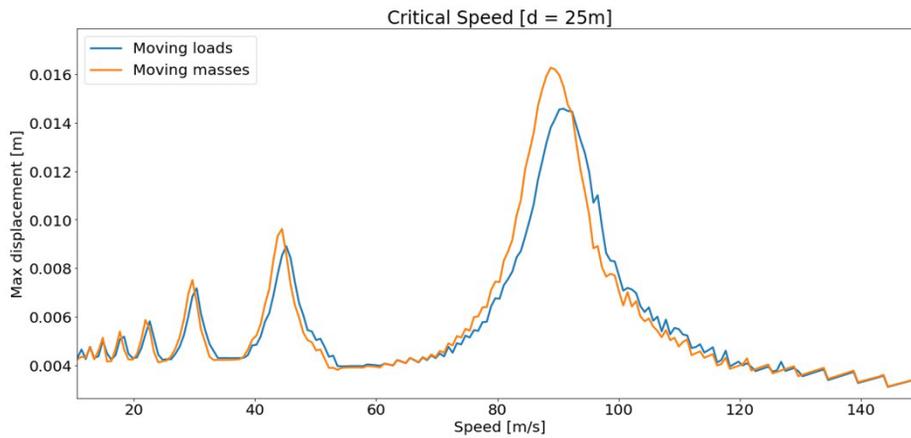
Figure 21. Critical speed analysis [d=25m]

The critical speeds (peaks) in Figure 21 seem to be shifted to the left when dealing with the moving masses analysis. This represents a decrease in critical speeds and can be coherently justified by the fact that the vehicle masses are being added to the system as a whole. Which in turn, evidently, decreases its natural frequencies and as a consequence, lower vehicle travelling (lower external frequency) speeds are able to generate maximum responses. The same train with a smaller distance *d* between axles would have generated a slightly greater left shift in the critical speeds, since the amount of masses that would have been present on the system at the same time would also have been greater as will be shown.
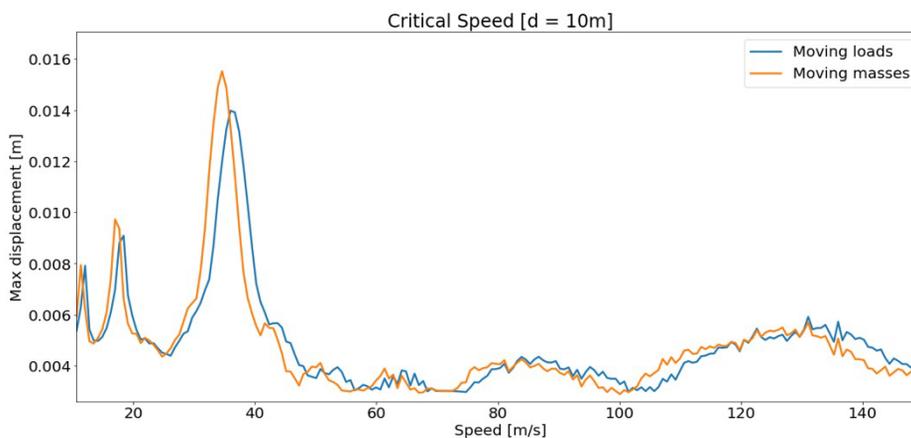
Figure 22. Critical speed analysis [d=10m]

Figure 22 shows that the main critical speed peak moved from 90 m/s in Figure 21 to approximately 40 m/s by simply changing the length of the vehicle. In both figures the moving mass analyses displacements show a greater value than the moving load analyses. Critical speeds are calculated for a specific set of vehicle and structure. Any change on the set leads to a completely different response behavior.

6 CONCLUSIONS

The bridge dynamic problem induced by moving bodies has been studied since the beginnings of engineering itself. Although it is common practice to adopt simplified and standardized methods to overcome these kinds of problem, the current technological development allows specific approaches to solve specific problems. This, in turn, may even generate more affordable solutions. One approach possibility is to include the inertial forces caused by the travelling vehicles in the analysis. Its relevance grows as the vehicle speed and/or the mass ratio grow.

The presented software solves the dynamic problem by coupling the vehicle mass matrix with the structure mass matrix at each integration time step. The problem formulation can be easily extended in order to account for two-dimensional finite elements, more complex vehicles, rail irregularities, jump conditions and so on.

As shown, for low mass ratios the responses difference magnitude between moving mass and load analyses stays negligible within engineering perspective. On the other hand, it was noticed that for mass ratios greater than one, the moving mass analysis should be chosen instead of the moving load one, since the absolute and the relative differences show values that cannot be treated as irrelevant any more. Additionally, the maximum relative and absolute difference do not occur at the same instant in the time-history analyses.

The consideration of the vehicle inertial forces in the analysis decreases the resonant speeds as the mass ratio increases in the overall scenario. This generates more precise and reliable results which tend to be closer to reality despite the inherent and necessary approximations.

Taking into account the technological resources currently available, the moving mass analysis might be more advantageous than the moving load analysis. In most cases, the amount of additional computational time and power required for the inertial analysis do not represent a major problem.

7 REFERENCES

[1] S. S. Lima, H. L. Soriano, and F. J. C. Reis, "Considerações quanto à determinação do coeficiente de impacto em pontes," *Eng. Estud. Pesqui.*, vol. 5, p. 7, 2002.

[2] F. K. R. Cepeda and F. G. Castillo, *Análisis Dinámico de Estructuras Sometidas a Acciones de Trenes de Alta Velocidad*. Madrid: Grupo de Mecánica Computacional/Universidad Politécnica de Madrid, 2005.

[3] E. Savin, "Dynamic amplification factor and response spectrum for the evaluation of vibrations of beams under successive moving loads," *J. Sound Vibrat.*, vol. 248, no. 2, pp. 267–288, 2001.

[4] L. Frýba, *Vibration of Solids and Structures under Moving Loads*. The Netherlands: Springer, 1972.

[5] L. Frýba and T. Telford, *Dynamics of Railway Bridges*. República Tcheca: Thomas Telford Ltd., 1996, pp. 332.

[6] S. P. Timoshenko, D. H. Young, and W. Weaver, *Vibration Problems in Engineering*. Baltimore: John Wiley & Sons, 1974.

[7] Y. B. Yang, J. D. Yau, and Y. S. Wu, *Vehicle-Bridge Interaction Dynamics: With Applications to High-Speed Railways*. Singapore: World Scientific Publishing Co. Pte. Ltd., 2004.

[8] Y. Wang, Q. Wei, J. Shi, and X. Long, "Resonance characteristics of two-span continuous beam under moving high speed trains," *Lat. Am. J. Solids Struct.*, vol. 7, pp. 185–199, 2010.

[9] W. Suijiang, "Numerical calculation of bridge seismic response considering beam-block colligion effect," *J. Constr.*, pp. 111–122, 2019.

[10] P. Bucinskas and L. V. Andersen, "Dynamic response of vehicle-bridge-soil system using lumped-parameter models for structure-soil interaction," *Comput. Struc.*, vol. 238, pp. 106270, 2020.

[11] A. Pesterev, "On asymptotics of the solution of the moving oscillator problem," *J. Sound Vibrat.*, vol. 260, no. 3, pp. 519–536, 2003.

[12] R. C. Hora, S. S. Lima, and S. H. C. Santos, "Avaliação da resposta dinâmica de uma ponte sob ação de massas móveis," Dissertação de mestrado, Univ. Fed. Rio Jan., Rio de Janeiro, Brasil, 2021.

[13] K.-J. Bathe, *Finite Element Procedures*. USA: Prentice-Hall, 1996.

[14] C. A. Felippa, *Introduction to Finite Element Methods*. Colorado: Department of Aerospace Engineering Sciences and Center for Aerospace Structures, University of Colorado, 2004. p. 612.

[15] A. K. Chopra, *Dynamics of Structures. Theory and Application to Earthquake Engineering*, 4th ed. USA: Prentice-Hall.

[16] R. W. Clough and J. Penzien, *Dynamics of Structures*. Berkeley, CA, McGraw-Hill College, 2003.

[17] S. S. Lima and S. H. C. Santos, *Análise Dinâmica das Estruturas, vol. 1*. Rio de Janeiro: Ciência Moderna, 2008.

[18] S. S. Lima, *Análise de Estruturas com Computadores*. Rio de Janeiro: Ciência Moderna, 2017.

[19] N. M. Newmark and S. P. Chan, *A Comparison of Numerical Methods for Analyzing the Dynamic Response of Structures*. Urbana, Illinois: University of Illinois, 1952.

[20] G. Noh and K.-J. Bathe, "For direct time integrations: a comparison of the Newmark and Bathe schemes," *Comput. Struc.*, vol. 225, pp. 1–12, 2019.

[21] J. S. Przemieniecki, *Theory of Matrix Structural Analysis*. New York: McGraw-Hill, 1968.

Rev. IBRACON Estrut. Mater., vol. 16, no. 6, e16601, 2023

18/18